THE JOURNAL OF PHYSICAL CHEMISTRY Letters

Letter

pubs.acs.org/JPCL

Unusual Metallic Microporous Boron Nitride Networks

Jun Dai,[†] Xiaojun Wu,*[,‡,§] Jinlong Yang,[§] and Xiao Cheng Zeng*[,†,§]

[†]Department of Chemistry and Nebraska Center for Materials and Nanoscience, University of Nebraska—Lincoln, Lincoln, Nebraska 68588, United States

[‡]CAS Key Lab of Materials for Energy Conversion, Department of Materials Science and Engineering and Hefei National Lab for Physical Science at Microscale and [§]Department of Chemical Physics and Hefei National Lab for Physical Science at Microscale, University of Science and Technology of China, Hefei, Anhui 230026, China

Supporting Information

ABSTRACT: Two metallic zeolite-like microporous BN crystals with all-sp^2 bonding networks are predicted from an unbiased structure search based on the particle-swarm optimization (PSO) algorithm in combination with first-principles density functional theory (DFT) calculations. The stabilities of both microporous structures are confirmed via the phonon spectrum analysis and Born−Oppenheimer molecular dynamics simulations with temperature control at 1000 K. The unusual metallicity for the microporous BN allotropes stems from the delocalized p electrons along the axial direction of the micropores. Both microporous BN structures entail large surface areas, ranging from 3200 to 3400 m^2/g. Moreover, the microporous BN structures show a preference toward organic molecule adsorption (e.g., the computed adsorption energy for CH_3CH_2OH is much more negative than that of H_2O). This preferential adsorption can be exploited for water cleaning, as demonstrated recently using porous boron BN nanosheets (*Nat. Commun.* **2013**, *4*, 1777).

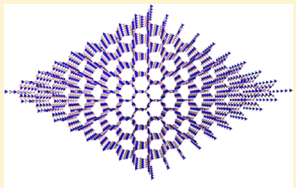

3-Dimensional BN Goes to Metallic

SECTION: Molecular Structure, Quantum Chemistry, and General Theory

Due to its ability to form sp-, sp^2-, and sp^3-hybridized covalent bonds, boron nitride (BN) exists in many different allotropic forms, such as three-dimensional (3D) BN crystals or amorphous BN,[1] two-dimensional (2D) sheets,[2−4] one-dimensional (1D) nanotubes,[4−6] and zero-dimensional (0D) nanocages.[7,8] In nature, 3D BN crystals can be classified into two types on the basis of their bonding behavior. The first type is graphite-like hexagonal (*h*-) and rhombohedral BN (*r*-BN), consisting of sp^2 bonded planes. The second type is diamond-like cubic (*c*-) and wurtzite BN (*w*-BN) with an sp^3 covalent network. The interlayer van der Waals interactions in the *h*-BN and *r*-BN structures render them compressible, whereas *c*-BN and *w*-BN structures belong to superhard materials due to the highly robust sp^3 networks. The *w*-BN structure was observed to possess extraordinarily high indentation hardness that rivals that of diamond.[9] Very recently, Tian et al. reported that nanotwinned *c*-BN is even harder than the synthetic diamond.[10] To date, it is generally believed that *c*-BN is the thermodynamically stable phase at ambient conditions while *h*-BN is more stable at high temperature.[11] Properties of various BN phases have been extensively studied from numerous theoretical calculations.[11−19] A number of new BN crystals have been predicted, such as *bct*-BN,[15,20] Z-BN,[17] P-BN,[18] B_4N_4 crystals,[19] and triangular BN foam.[21] Static first-principles calculations[14−16,22] and metadynamics simulations[20] were also undertaken to explore phase transformations in 3D BN. A possible transition pathway from *h*-BN to *bct*-BN at relatively high temperatures was proposed by Hromadová et al. based on a metadynamics simulation, and it was also found that *h*-BN tends to transform into *w*-BN at low temperatures.[20]

Despite their structural diversity, all 3D BN allotropes reported thus far possess a sizable band gap. The sp^3 bonded BN crystals usually exhibit a band gap of ∼4−6 eV.[12,18] In layered BN materials, the partially ionic sp^2-hybridized in-plane bonding also gives rise to a wide band gap (∼4.0−4.4 eV).[18] To date, the fully sp^2-hybridized nonlayered B_4N_4-II[18] and triangular BN[21] foam possess the narrowest band gaps among BN crystals, which are 1.33 and 1.35 eV, respectively. In addition, both 1D BN nanotubes and 2D nanosheets possess a wide band gap of ∼5−6 eV.[5] Bare armchair BN nanoribbons (BNNRs) are predicted to be wide-gap semiconductors, with band gaps ranging from 3.8 to 4.3 eV (depending on the width of the nanoribbon).[23] Although bare zigzag BNNRs are metals, as confirmed by both theoretical calculations and experimental measurements,[23−27] the dangling bonds at the edges are highly reactive and can be easily passivated. If both edges are passivated with hydrogen, zigzag BNNRs become nonmagnetic semiconductors, while selected hydrogenation of the B-edge of zigzag BNNRs may lead to half-metals.[28−32] Moreover, partial hydrogenation,[25] fluorination,[33,34] and oxygen passivation[35] can also lead to half-metallicity for zigzag BNNRs. Cubic BN(111) nanofilms can be turned into metallic when the (111) surface is passivated by hydrogen.[36]

A hitherto unanswered question is whether metallic BN crystals can exist. To address this question, we carry out a global structure search based on a particle-swarm optimization

Received: September 3, 2013
Accepted: September 30, 2013
Published: September 30, 2013

(PSO) algorithm[37] in combination with the first-principles density functional calculations to seek the possibility of metallic BN crystals. For the first time, theoretical evidence of metallic BN crystals with all-sp^2 bonding networks is shown. The structure stability of the metallic BN crystals is confirmed by both phonon spectrum analysis and high-temperature Born–Oppenheimer molecular dynamics (BOMD) simulations. The new BN crystals not only exhibit intriguing all-sp^2 zeolite-like structures and unusual metallicity but also show preferential adsorption of organic molecules (compared to water adsorption).

Geometrical Properties. After an extensive PSO structure search, two new microporous BN allotropes (see Figure 1) are

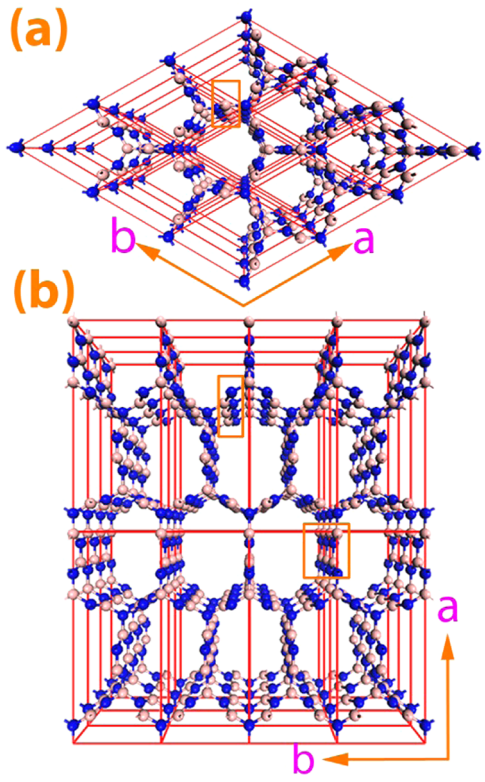

Figure 1. Optimized structures of the (a) (P-6M2)-BN and (b) (IMM2)-BN. Blue and pink spheres are nitrogen and boron atoms, respectively. The zigzag chains are highlighted by orange lines.

identified and predicted to be possibly metallic. Both BN allotropes share some special structural features, that is, both possess all-sp^2 bonded networks but with sizable pores within the networks. Note the all-sp^2 bonded structures are different from the ones predicted by applying transverse pressure on BNNTs, which exhibit either layered a porous structure or an sp^2–sp^3 bonded 3D structure.[38] They are also different from the recently predicted 3D carbon nanotube (CNT) polymers in which the CNTs are connected by sp^3 carbon.[39] The new BN structures have space groups of P-6M2 and IMM2, respectively; hereafter, they are named as the (P-6M2)-BN and (IMM2)-BN for discussions. The optimized lattice parameters (based on LDA) are a = 6.344 Å and c = 2.479 Å for the (P-6M2)-BN and a = 6.345 Å, b = 2.480 Å, and c = 15.307 Å for (IMM2)-BN, and the average volumes are 10.8 and 12.05 $Å^3$/atom for the (P-6M2)-BN and (IMM2)-BN, respectively. The (P-6M2)-BN can be viewed as 1-zBNNRs (see ref 40 for details of this notion) fused by sp^2 B or N, forming hexagon-like pores, while the (IMM2)-BN can be viewed as 1-zBNNRs and 2-zBNNRs alternatively connected by sp^2 B or N, forming slightly larger hexagonal pores than the (P-6M2)-BN. Due to these unique structural properties, direct conversion of layered *r*-BN or *h*-BN to the new BN allotropes may be very difficult. However, a combination of the template-assisted technique with functionalized narrow zigzag BNNRs can be a plausible way.

Stabilities. To confirm the structural stability of the (P-6M2)-BN and (IMM2)-BN, the dynamic stability is examined first through phonon spectrum calculations. As shown in Figure 2,

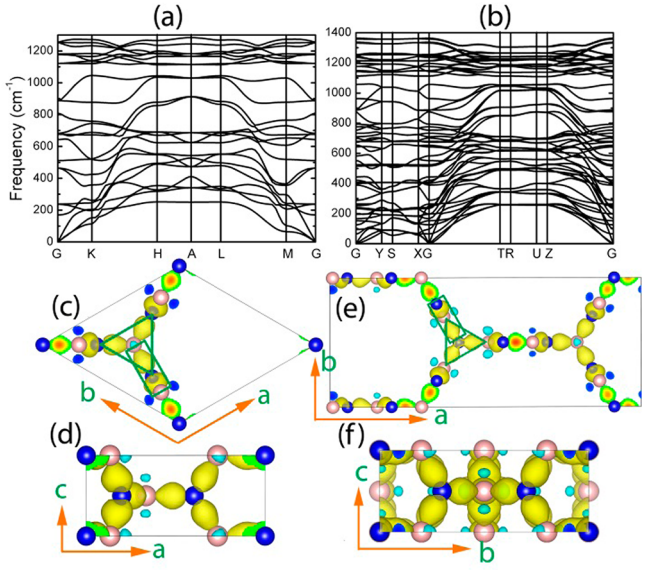

Figure 2. Phonon band structures of the (a) (P-6M2)-BN, (b) (IMM2)-BN. G(0.0, 0.0, 0.0), K(1/3, 1/3, 0.0), H(1/3, 1/3, 0.5), A(0.0, 0.0, 0.5), L(0.5, 0.0, 0.5), M(0.5, 0.0, 0.0), Y(0.0, 0.5, 0.0), S(0.5, 0.5, 0.0), X(0.5, 0.0, 0.0), T(0.0, 0.5, 0.5) R(0.5, 0.5, 0.5), U(0.5, 0.0, 0.5), and Z(0.0, 0.0, 0.5) refer to special points in the first Brouillon zone. (c–f) The isosurfaces of the charge density difference with an isovalue of 0.025 e/au for the (P-6M2)-BN (c,d) and (IMM2)-BN (e,f) from different perspectives. Yellow and cyan regions refer to electron-rich and -deficient regions, respectively. The green triangles and rectangles denote the adjacent perpendicular sp^2 units.

no imaginary phonon frequencies are observed in the Brillouin zone for both the (P-6M2)-BN and (IMM2)-BN, indicating inherent dynamical stability of both new BN allotropes. Note that at low temperature, the atomic motions in the crystal can be decomposed into nearly independent phonon modes (normal modes); therefore, the phonon instability is both the necessary and sufficient condition for mechanical instability of a crystal at low temperature. The highest frequencies at the zone center G point are 1255 and 1363 cm^{-1} for the (P-6M2)-BN and (IMM2)-BN, respectively, close to 1299 cm^{-1} for the bulk *h*-BN,[41] suggesting strong B–N bonding. We have also performed BOMD simulations to examine the thermal stability of the new BN allotropes at an elevated temperature. The constant-temperature and -volume (*NVT*) and constant-temperature and -pressure (*NPT*) ensembles are adopted. The time step is 3 fs, and the total simulation time is 12 ps for the given temperature (1000 K). We find that the structural integrity is well kept for both the (P-6M2)-BN and (IMM2)-BN (see Supporting Information Figure S1 and movies based on the *NPT* ensemble simulation), suggesting high thermal stability for both network structures. The cohesive energy is

dx.doi.org/10.1021/jz4018877 | *J. Phys. Chem. Lett.* 2013, 4, 3484–3488

defined by the formula $E_{coh} = (nE_B + nE_N - E_{(BN)_n})/n$, in which E_B, E_N, and $E_{(BN)_n}$ are the total energies of a single B atom, a single N atom, and a $(BN)_n$ compound, respectively. We find that the cohesive energies of the predicted (P-6M2)-BN and (IMM2)-BN are greater than that of NiAs-type BN. Because LDA can be inaccurate to compute the atomization energy, we also compute the cohesive energy using the HSE06 hybrid functional. Again, the computed cohesive energies of (P-6M2)-BN and (IMM2)-BN are greater than that of the NiAs-type BN (see Supporting Information Table S1).

To achieve a better understanding of the high stability of the systems, we also analyze the bonding properties of both BN allotropes through computing the deformation electronic density, as shown in Figure 2c–f. The deformation electronic density is defined as the total electronic density excluding the superposition of atomic charge density. We can clearly see that the B–N covalent bond is a polar bond, and the major part of the electron-rich area is closer to N. Each B (N) is bonded with three N (B) atoms, reflecting the sp^2 feature. If every three neighboring B–N bonds are viewed as an sp^2 unit, one can see in the (P-6M2)-BN that every sp^2 unit is connected by another sp^2 unit perpendicular to it with a sharing B–N bond. The same feature also appears in the joint regions of the micropores and the areas with 1-zBNNRs (as highlighted by green triangles and rectangles in Figure 2c and e). The adjacent perpendicular sp^2 unit may help to stabilize the system because the interaction between the electrons in the *ab* plane and the electrons in the plane perpendicular to it is minimized in all sp^2 networks.

Electronic Properties. The electronic band structures of the (P-6M2)-BN and (IMM2)-BN are shown in Figure 3a and b.

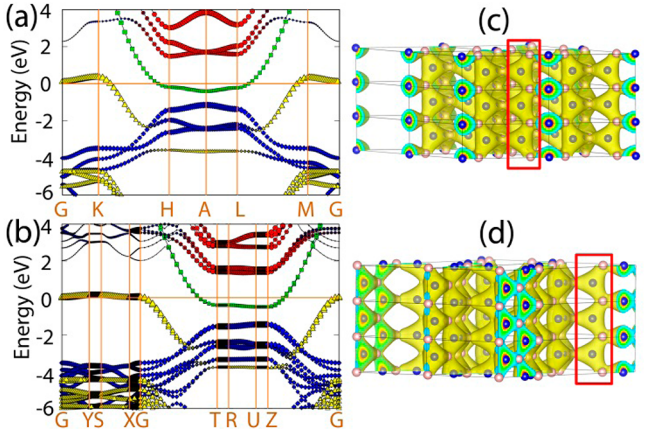

Figure 3. Electronic band structures of (a) (P-6M2)-BN and (b) (IMM2)-BN. The sizes of the red circles, green squares, blue diamonds, and yellow triangles denote the contribution of $s + p_x + p_y$ states of B, p_z states of B, $s + p_x + p_y$ states of N, and p_z states of N. The Fermi energy is set to zero. Isosurface of charge density with an isovalue of 0.1 e/au for (c) (P-6M2)-BN and (d) (IMM2)-BN.

Clearly, for the (P-6M2)-BN, the p_z band of N crosses the Fermi level at around K and M, and the p_z band of B crosses the Fermi level at around H and L, while for the (IMM2)-BN, the same feature appears at around G for the p_z band of N and along G–T and Z–G for the p_z band of B, showing a metallic characteristic. Besides, the N p_z band is quite flat along the G–K and M–G for the (P-6M2)-BN and along the G–Y–S–X–G for the (IMM2)-BN, and the B p_z band is also quite flat along the H–A–L for the (P-6M2)-BN and along the T–R–U–Z for the (IMM2)-BN. These features indicate that the p_z electrons in the *ab* plane are quite localized. This can be understood as a result of the existence of sizable pores and the perpendicular adjacent sp^2 units in these systems. However, along the *c* direction, the p_z bands are highly delocalized, with appreciable dispersions along the K–H and L–M for the (P-6M2)-BN and along the G–T and Z–G for the (IMM2)-BN. The delocalized p_z electrons along the *c* direction result in long-range conductive channels along the *c* direction (see Figure 3c and d), making these systems metallic. Because the LDA tends to underestimate the band gaps for semiconductors and sometimes incorrectly predicts a metal, the electronic structures of both new BN allotropes are also computed using the more accurate hybrid HSE06 functional;[42] the computed band gaps of the monolayer BN and *h*-BN based on the HSE06 function are 5.69 and 5.57 eV, respectively, and are in agreement with the experimental results, indicating reliability of HSE06 for the BN systems. As shown in Figure S2 (Supporting Information), the metallic feature also arises based on the HSE06 computation. Therefore, we believe that the predicted metallicity from the LDA is reliable.

Potential Applications for Water Cleaning. Porous BN materials have attracted much attention due to their potential applications as effective adsorbent materials.[43−46] Because BN is composed of light elements, BN adsorbents typically have high-uptake gravimetric capacity. BN materials also exhibit high thermal and chemical stability, a highly desirable feature for recycling. Moreover, the partial ionic bonds and high specific surface area render the porous BN materials effective adsorbents for various chemicals such as oils, organic solvents, dynes,[45] and hydrogen.[46] In the current form, both microporous BN structures entail large surface areas greater than 3000 m^2/g. More specifically, the surface areas of (P-6M2)-BN and (IMM2)-BN are 3375 and 3229 m^2/g, respectively. To assess the possibility for water filtering, we compute adsorption energies of H_2O, CH_3CH_2OH (ethanol), and CO_2 within the porous BN materials (the adsorption structures can be found in Figure S3, Supporting Information). Here, the adsorption energy is defined as $E_{ad} = E_{a+b} - E_a - E_b$, where E_{a+b} is the total energy of the porous BN material with the adsorbate and E_a and E_b are the total energies of the porous BN material and adsorbate, respectively. The adsorption energies computed with or without the Grimme's D2 dispersion correction[47] are summarized in Table 1. Both newly predicted porous BN materials exhibit a notable preference toward the ethanol adsorption, compared to water. Thus, the predicted porous BN materials may be used for removal of trace amounts of organic molecules from water. Indeed, porous BN nanosheets have been recently demonstrated to have remarkable water-cleaning capability.[45]

Table 1. Computed Adsorption Energies of H_2O, CH_3CH_2OH, and CO_2 on (P-6M2)-BN and (IMM2)-BN with or without Grimme's D2 Dispersion (vdW) Correction[a]

	(P-6M2)-BN with vdW	(P-6M2)-BN w/o vdW	(IMM2)-BN with vdW	(IMM2)-BN w/o vdW
H_2O	−1.07	−0.58	−0.62	−0.19
CH_3CH_2OH	**−2.21**	−0.52	**−1.82**	−0.53
CO_2	−1.28	−0.48	−0.90	−0.48

[a]The unit of the adsorption energy is eV.

dx.doi.org/10.1021/jz4018877 | J. Phys. Chem. Lett. 2013, 4, 3484−3488

In conclusion, we predict two novel metallic BN allotropes with microporous structures and all-sp^2 bonded networks, namely, (P-6M2)-BN and (IMM2)-BN. Stabilities of both systems are confirmed by phonon spectrum calculations and BOMD simulations. The metallicity is attributed to the delocalized p electrons along the axial direction of the zeolite-like micropores. The new BN allotropes are not only conceptually fascinating due to their highly stable all-sp^2 bonded networks, anisotropic metallicity, high-temperature stability, and large surface areas (>3000 m^2/g), but they are also promising for applications such as gas storage, separation, and filtering under extreme environments. If confirmed by experiments, the microporous BN structures will undoubtedly enrich the existing family of 3D BN materials in both structure and functionality.

COMPUTATIONAL DETAILS

The structure search is performed using the PSO algorithm within the evolutionary scheme as implemented in the CALYPSO (Crystal structure AnaLYsis by Particle Swarm Optimization) code.[37] PSO offers an efficient and fast way to obtain reliable structures with the input of chemical composition only. Another advantage of the PSO algorithm is that it requires few parameters to adjust. The effectiveness of this algorithm has been demonstrated in its successful prediction of various high-pressure and low-dimensional structures.[48−54] BN with 2−8 formula units in a unit cell have been searched using the algorithm. In our structure search, the population size is set to be 30, and the number of generation is maintained to 30. As a result, a total number of 6300 configurations are examined to ensure the unbiased structure search. In the first generation, random structures are constructed by generating atomic coordinates using crystallographic symmetry operations. Next, the structures are optimized using a density functional theory (DFT) method (see below). Third, the best 60% structures are selected by PSO to generate the next generation; other structures in the new generation are generated randomly, which guarantees the structural diversity. The local structure relaxations and electronic band structure calculations are performed in the framework of DFT as implemented in the VASP package.[55] Local density approximation (LDA) is adopted to treat the exchange−correlation energy. The ion−electron interaction is treated using the projector augment wave (PAW) technique. For geometric optimization, both lattice constants and atomic positions are relaxed until the forces on the atoms are less than 0.02 eV/Å and the total energy change is less than 1.0×10^{-5} eV. For geometrical relaxation, the Brillouin zone is sampled using k-points with 0.02 $Å^{-1}$ spacing in the Monkhorst−Pack scheme,[56] while for the density of states, a denser k-points grid with 0.01 $Å^{-1}$ spacing is used. Phonon spectrum calculations are performed using the density functional perturbation theory as implemented in the Quantum-Espresso package.[57]

ASSOCIATED CONTENT

Supporting Information

Cohesive energies of new BN allotropes, the $B_{12}N_{12}$ cage, some typical BNNTs and known bulk BN crystals, snapshots of the (P-6M2)-BN and (IMM2)-BN after a 12 ps BOMD simulation at 1000 K, HSE06 band structures of the (P-6M2)-BN and (IMM2)-BN, and adsorption structures of H_2O, CO_2, and CH_3CH_2OH on (P-6M2)-BN and (IMM2)-BN. This material is available free of charge via the Internet at http://pubs.acs.org.

AUTHOR INFORMATION

Corresponding Authors

*E-mail: zeng1@unl.edu (X.C.Z.).
*E-mail: xjwu@ustc.edu.cn (X.W.).

Notes

The authors declare no competing financial interest.

ACKNOWLEDGMENTS

The USTC group is supported by the National Basic Research Programs of China (Nos. 2011CB921400, 2012CB 922001), NSFC (Grant 21121003, 11004180, 51172223), the One Hundred Person Project of CAS, the Strategic Priority Research Program of CAS (XDB01020300), the Shanghai Supercomputer Center, and the Hefei Supercomputer Center. The UNL group is supported by the ARL (Grant W911NF1020099), NSF (Grant DMR-0820521), and a grant from USTC for (1000plan) Qianren-B summer research.

REFERENCES

(1) Haubner, R.; Wilhelm, M.; Weissenbacher, R.; Lux, B. *Boron Nitrides—Properties, Synthesis and Applications*; Springer: Berlin, Germany, 2002.
(2) Pacilé, D.; Meyer, J. C.; Girit, C. O.; Zettl, A. The Two-Dimensional Phase of Boron Nitride: Few-Atomic-Layer Sheets and Suspended Membranes. *Appl. Phys. Lett.* **2008**, *92*, 133107/1−133107/3.
(3) Corso, M.; Auwärter, W.; Muntwiler, M.; Tamai, A.; Greber, T.; Osterwaler, J. Boron Nitride Nanomesh. *Science* **2004**, *303*, 217−220.
(4) Golberg, D.; Bando, Y.; Huang, Y.; Terao, T.; Mitome, M.; Tang, C. Boron Nitride Nanotubes and Nanosheets. *ACS Nano* **2010**, *4*, 2979−2993.
(5) Rubio, A.; Corkill, J. L.; Cohen, M. L. Theory of Graphic Boron Nitride Nanotubes. *Phys. Rev. B* **1994**, *49*, 5081−5084.
(6) Chopra, N. G.; Luyken, R. J.; Cherrey, K.; Crespi, V. H.; Cohen, M. L.; Louie, S. G.; Zettl, A. Boron Nitride Nanotubes. *Science* **1995**, *269*, 966−967.
(7) Stéphen, O.; Bando, Y.; Loiseau, A.; Willamie, F.; Shramchenko, N.; Tamiya, T.; Sato, T. Formation of Small Single-Layer and Nested BN Cages under Electron Irradiation of Nanotubes and Bulk Material. *Appl. Phys. A: Mater. Sci. Process.* **1998**, *67*, 107−111.
(8) Golberg, D.; Bando, Y.; Stéphen, O.; Kurashima, K. Octahedral Boron Nitride Fullerenes Formed by Electron Beam Irradiation. *App. Phys. Lett.* **1998**, *73*, 2441−2443.
(9) Dubrovinskaia, N.; Solozhenko, V. L.; Miyajima, N.; Dmitriev, V.; Kurakevych, O. O.; Dubrovinsky, L. Superhard Nanocomposite of Dense Polymorphs of Boron Nitride: Nanocarbon Material Has Reached Diamond Hardness. *Appl. Phys. Lett.* **2007**, *90*, 101912/1−101912/3.
(10) Tian, Y.; Xu, B.; Yu, D.; Ma, Y.; Wang, Y.; Jiang, Y.; Hu, W.; Tang, C.; Gao, Y.; Luo, K.; et al. Ultrahard Nanotwinned Cubic Boron Nitride. *Nature* **2013**, *493*, 385−388.
(11) Kern, G.; Kresse, G.; Hafner, J. Ab Initio Calculation of the Lattice Dynamics and Phase Diagram of Boron Nitride. *Phys. Rev. B* **1999**, *59*, 8551−8559.
(12) Furthmüller, J.; Hafner, J.; Kressem, G. Ab Initio Calculation of the Structural and Electronic Properties of Carbon and Boron Nitride Using Ultrasoft Pseudopotentials. *Phys. Rev. B* **1994**, *50*, 15606−15622.
(13) Albe, K. Theoretical Study of Boron Nitride Modifications at Hydrostatic Pressure. *Phys. Rev. B* **1997**, *55*, 6203−6210.
(14) Yu, W. J.; Lau, W. M.; Chan, S. P.; Liu, Z. F.; Zheng, Q. Q. Ab Initio Study of Phase Transformations in Boron Nitride. *Phys. Rev. B* **2003**, *67*, 014108/1−014108/9.
(15) Wen, B.; Zhao, J.; Melnik, R.; Tian, Y. Body-Centered Tetragonal B_2N_2: A Novel sp^3 Bonding Boron Nitride Polymorph. *Phys. Chem. Chem. Phys.* **2011**, *13*, 14565−14570.

(16) Li, Z.; Gao, F. Structure, Bonding, Vibration and Ideal Strength of Primitive-Centered Tetragonal Boron Nitride. *Phys. Chem. Chem. Phys.* **2012**, *14*, 869−876.
(17) He, C.; Sun, L.; Zhang, C.; Peng, X.; Zhang, K.; Zhong, J. Z-BN: A Novel Superhard Boron Nitride Phase. *Phys. Chem. Chem. Phys.* **2012**, *14*, 10967−10971.
(18) Jiang, X.; Zhao, J.; Ahuja, R. A Novel Superhard BN Allotrope under Cold Compression of h-BN. *J. Phys: Condens. Matter* **2013**, *25*, 122204/1−122204/6.
(19) Germaneau, É.; Su, G.; Zheng, Q. R. New Boron Nitride Structures B_4N_4: A First-Principles Random Searching Application. *J. Phys: Condens. Matter* **2013**, *25*, 125504/1−125504/10.
(20) Hromadová, L.; Martoňák, R. Pressure-Induced Structural Transitions in BN from Ab Initio Metadynamics. *Phys. Rev. B* **2011**, *84*, 224108/1−224108/7.
(21) Wu, M.; Wu, X.; Pei, Y.; Wang, Y.; Zeng, X. C. Three-Dimensional Network Model of Carbon Containing Only sp^2-Carbon Bonds and Boron Nitride Analogues. *Chem. Commun.* **2011**, *47*, 4406−4408.
(22) Wentzcovitch, R. M.; Fahy, S.; Cohen, M. L.; Louie, S. G. Ab Initio Study of Graphite-Diamondlike Transitions in BN. *Phys. Rev. B* **1988**, *38*, 6191−6195.
(23) Topsakai, M.; Aktürk, E.; Ciraci, S. First-Principles Study of Two- and One-Dimensional Honeycomb Structures of Boron Nitride. *Phys. Rev. B* **2009**, *79*, 115442/1−115442/11.
(24) Zeng, H.; Zhi, C.; Zhang, Z.; Wei, X.; Wang, X.; Guo, W.; Bando, Y.; Golberg, D. "White Graphenes": Boron Nitride Nanoribbons via Boron Nitride Nanotube Unwrapping. *Nano Lett.* **2010**, *10*, 5049−5055.
(25) Chen, W.; Li, Y.; Yu, G.; Li, C.; Zhang, S.; Zhou, Z.; Chen, Z. Hydrogenation: A Simple Approach To Realize Semiconductor−Half-Metal−Metal Transition in Boron Nitride Nanoribbons. *J. Am. Chem. Soc.* **2010**, *132*, 1699−1705.
(26) Zhang, Z.; Guo, W. Energy-Gap Modulation of BN Ribbons by Transverse Electric Fields: First-Principles calculations. *Phys. Rev. B* **2008**, *77*, 075403/1−075403/5.
(27) Zhang, Z.; Guo, W.; Yakobson, B. I. Self-Modulated Band Gap in Boron Nitride Nanoribbons and Hydrogenated Sheets. *Nanoscale* **2013**, *5*, 6381−6387.
(28) Zheng, F. W.; Zhou, G.; Liu, Z. R.; Wu, J.; Duan, W. H.; Gu, B. L.; Zhang, S. B. Half Metallicity along the Edge of Zigzag Boron Nitride Nanoribbons. *Phys. Rev. B* **2008**, *78*, 205415/1−205415/5.
(29) Barone, V.; Peralta, J. E. Magnetic Boron Nitride Nanoribbons with Tunable Electronic Properties. *Nano Lett.* **2008**, *8*, 2210−2214.
(30) Wu, M.; Wu, X.; Pei, Y.; Zeng, X. Inorganic Nanoribbons with Unpassivated Zigzag Edges: Half Metallicity and Edge Reconstruction. *Nano Res.* **2011**, *4*, 233−239.
(31) Lai, L.; Lu, J.; Wang, L.; Luo, G. F.; Zhou, J.; Qin, R.; Gao, Z. X.; Mei, W. N. Magnetic Properties of Fully Bare and Half-Bare Boron Nitride Nanoribbons. *J. Phys. Chem. C* **2009**, *113*, 2273−2276.
(32) Kan, E.; Wu, F.; Xiang, H. J.; Yang, J. L.; Whangbo, M.-H. Half-Metallic Dirac Point in B-Edge Hydrogenated BN Nanoribbons. *J. Phys. Chem. C* **2011**, *115*, 17252−17254.
(33) Wang, Y. L.; Ding, Y.; Ni, J. Fluorination-Induced Half-Metallicity in Zigzag Boron Nitride Nanoribbons: First-Principles Calculations. *Phys. Rev. B* **2010**, *81*, 193407/1−193407/4.
(34) Zhang, Z.; Zeng, X. C.; Guo, W. L. Fluorinating Hexagonal Boron Nitride into Diamond-Like Nanofilms with Tunable Band Gap and Ferromagnetism. *J. Am. Chem. Soc.* **2011**, *133*, 14831−14838.
(35) Lopez-Bezanilla, A.; Huang, J. S.; Terrones, H.; Sumpter, B. G. Boron Nitride Nanoribbons Become Metallic. *Nano Lett.* **2011**, *11*, 3267−3273.
(36) Zhang, Z. H.; Guo, W. L. Intrinsic Metallic and Semiconducting Cubic Boron Nitride Nanofilms. *Nano Lett.* **2012**, *12*, 3650−3655.
(37) Wang, Y.; Lv, J.; Zhu, L.; Ma, Y. CALYPSO: A Method for Crystal Structure Prediction. *Comput. Phys. Commun.* **2012**, *183*, 2063−2070.
(38) Hao, S.; Zhou, G.; Duan, W.; Wu, J.; Gu, B. L. Transverse Pressure Induced Phase Transitions in Boron Nitride Nanotube Bundles and the Lightest Boron Nitride Crystal. *J. Am. Chem. Soc.* **2008**, *130*, 5257−5261.
(39) Zhao, Z.; Xu, B.; Wang, L. M.; Zhou, X. F.; He, J.; Liu, Z.; Wang, H. T.; Tian, Y. Three Dimensional Carbon-Nanotube Polymers. *ACS Nano* **2011**, *5*, 7226−7234.
(40) Park, C.; Louie, S. G. Energy Gaps and Stark Effect in Boron Nitride Nanoribbons. *Nano Lett.* **2008**, *8*, 2200−2203.
(41) Miyamoto, Y.; Cohen, M. L.; Louie, S. G. Ab Initio Calculation of Phonon Spectra for Graphite, BN and BC_2N Sheets. *Phys. Rev. B* **1995**, *52*, 14971−14975.
(42) Heyd, J.; Scuseria, G. E.; Ernzerhof, M. Erratum: "Hybrid Functionals Based on A Screened Coulomb Potential". *J. Chem. Phys.* **2006**, *124*, 219906.
(43) Vinu, A.; Terrones, M.; Golberg, D.; Hishita, S.; Ariga, K.; Mori, T. Synthesis of Mesoporous BN and BCN Exhibiting Large Surface Areas via Templating Methods. *Chem. Mater.* **2005**, *17*, 5887−5890.
(44) Dibandjo, P.; Bois, L.; Chassagneux, F.; Cornu, D.; Letoffe, J. M.; Toury, B.; Babonneau, F.; Miele, P. Synthesis of Boron Nitride with Ordered Mesostructure. *Adv. Mater.* **2005**, *17*, 571−574.
(45) Lei, W.; Portehault, D.; Liu, D.; Qin, S.; Chen, Y. Porous Boron Nitride Nanosheets for Effective Water Cleaning. *Nat. Commun.* **2013**, *4*, 1777/1−1777/7.
(46) Weng, Q.; Wang, X.; Zhi, C.; Bando, Y.; Golberg, D. Boron Nitride Porous Microbelts for Hydrogen Storage. *ACS Nano* **2013**, *7*, 1558−1565.
(47) Grimme, S. Semiempirical GGA-Type Density Functional Constructed with a Long-Range Dispersion Correction. *J. Comput. Chem.* **2006**, *27*, 1787−1799.
(48) Zhu, L.; Wang, H.; Wang, Y.; Lv, J.; Ma, Y.; Cui, Q.; Ma, Y.; Zou, G. Substitutional Alloy of Bi and Te at High Pressure. *Phys. Rev. Lett.* **2011**, *106*, 145501/1−145501/4.
(49) Lv, J.; Wang, Y.; Zhu, L.; Ma, Y. Predicted Novel High-Pressure Phases of Lithium. *Phys. Rev. Lett.* **2011**, *106*, 015503/1−015503/4.
(50) Zhu, L.; Wang, Z.; Wang, Y.; Zou, G.; Mao, H.; Ma, Y. Spiral Chain O_4 Form of Dense Oxygen. *Proc. Natl. Acad. Sci. U.S.A.* **2012**, *109*, 751−753.
(51) Wang, Y.; Liu, H.; Lv, J.; Zhu, L.; Wang, H.; Ma, Y. High Pressure Partially Ionic Phase of Water Ice. *Nat. Commum.* **2011**, *2*, 563/1−563/5.
(52) Luo, X.; Yang, J.; Liu, H.; Wu, X.; Wang, Y.; Ma, Y.; Wei, S. H.; Gong, X.; Xiang, H. Predicting Two-Dimensional Boron−Carbon Compounds by the Global Optimization Method. *J. Am. Chem. Soc.* **2011**, *133*, 16285−16290.
(53) Wu, X.; Dai, J.; Zhao, Y.; Zhuo, Z.; Yang, J.; Zeng, X. C. Two-Dimensional Boron Monolayer Sheets. *ACS Nano* **2012**, *6*, 7443−7453.
(54) Dai, J.; Zhao, Y.; Wu, X.; Zeng, X. C. Exploration of Structures of Two-Dimensional Boron−Silicon Compounds with sp^2 Silicon. *J. Phys. Chem. Lett.* **2013**, *4*, 561−567.
(55) Kresse, G.; Furthmüller, J. Efficient Iterative Schemes For Ab Initio Total-Energy Calculations Using a Plane-Wave Basis Set. *Phys. Rev. B* **1996**, *54*, 11169−11186.
(56) Monkhorst, H. J.; Pack, J. D. Special Points for Brillouin-Zone Integrations. *Phys. Rev. B* **1976**, *13*, 5188−5192.
(57) Giannozzi, P.; Baroni, S.; Bonini, N.; Calandra, M.; Car, R.; Cavazzoni, C.; Ceresoli, D.; Chiarotti, G. L.; Cococcioni, M.; Dabo, I.; et al. QUANTUM ESPRESSO: A Modular and Open-Source Software Project for Quantum Simulations of Materials. *J. Phys.: Condens. Matter* **2009**, *21*, 395502/1−395502/19.